Organic & Biomolecular Chemistry

Symmetrically Backfolded Molecules Emulating the Self-Similar Features of Sierpinski Triangle

Journal:	*Organic & Biomolecular Chemistry*
Manuscript ID	OB-COM-04-2019-000958.R1
Article Type:	Paper
Date Submitted by the Author:	16-May-2019
Complete List of Authors:	Hu, Jie-Ying; Guangdong University of Technology, School of Chemical Engineering and Light Industry Guangzhou Higher Education Mega Center Sun, Yanqiong; Fuzhou University XIAO, Ran; City University of Hong Kong Cheng, Sheng-Xian; City University of Hong Kong College of Science and Engineering, He, Jun; Guangdong University of Technology, School of Chemical Engineering and Light Industry Zeller, Matthias; Purdue University Wong, Wai-Yeung ; Hong Kong Baptist University Xu, Zhengtao; City University of Hong Kong, Department of Chemistry

ARTICLE

Symmetrically Backfolded Molecules Emulating the Self-Similar Features of Sierpinski Triangle†

Received 00th January 20xx,
Accepted 00th January 20xx

DOI: 10.1039/x0xx00000x

Jieying Hu,[a] Yan-Qiong Sun,[b] Ran Xiao,[c] Shengxian Cheng,[c] Jun He,*[a] Matthias Zeller,[d] Wai-Yeung Wong,*[e] and Zhengtao Xu*[c]

We synthesize self-similar molecules (**G3** and **G2**; based on phenylalkynyl backbones) with symmetrically backfolded shapes inspired by the famous fractal of the Sierpinski triangle. Unlike the more traditional, starburst dendrimers, the centripetal-shaped Sierpinski molecules feature side branches symmetrically bent away from the growth direction of the main branch, thus contrasting the natural-tree shape. Molecule **G3** exhibits three distinct levels of structural hierarchy comprising the primary, secondary and tertiary branches, while the smaller **G2** contains only features of the 1st and 2nd orders. In spite of the much larger conjugated backbone of **G3**, its solution UV-vis absorption and fluorescence exhibits no red shift relative to **G2**. In a test of nitrobenzene sensing, the thin film of G3 deposited from THF was more sensitively quenched in fluorescence than the smaller **G2**.

Introduction

The relevance of the mathematically famous fractal of the Sierpinski triangle to molecular design is illustrated in Fig. 1. The hierarchy (or iteration) of the triangles is superimposable with a ternary tree that features a symmetrically backfolded geometry,[1-5] in which the subbranches are bent away from the pointing direction of the main branches. Such a backfolded geometry contrasts with the starburst shape of conventional dendrimers, with all branches in the latter radiating away from the center (e.g., H_6**L3**; Fig. 1), mimicking the growth direction of a biological tree. Even though symmetrically backfolded molecules have been studied by chemists (e.g., **L1** and **L2** in Fig. 1 and other examples[6-12]), most examples remain rather simple systems consisting of only primary and secondary branches (e.g., **L1** and **L2**). The synthesis of Sierpinski molecules of higher iterations (e.g., **G3** in Fig. 2, with three generations of branches) has not been reported.

The lack of synthetic efforts on higher-generation Sierpinski molecules is curious, and stands in sharp contrast not only with the numerous reports on conventional dendrimers of the radiating, starburst shape,[13-20] but with the growing numbers of supramolecular assemblies related to the Sierpinski fractal.[21-28] On a more technical plane, the backfolded shape of Sierpinski molecules offers unique opportunities in molecular design (as outlined in earlier works).[1-5, 29] A comparison of backfolded **L2** and starburst H_6**L3** is illustrative. While the end groups of H_6**L3** consist of six chemically equivalent, separate carboxyl groups, **L2** offers two sets of terminal sites: the –CN groups on the three

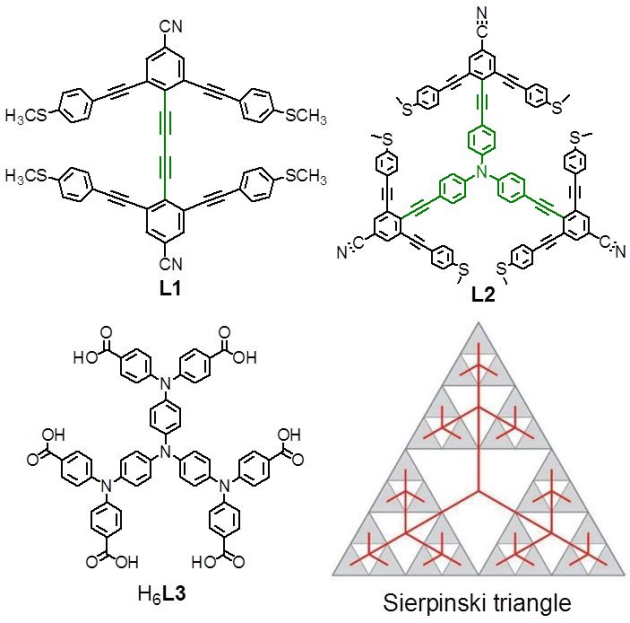

Fig. 1 Two backfolded molecules (**L1** and **L2**), the starburst dendrimer H_6**L3**, and a Sierpinski triangle (with the equivalent ternary tree shown in red). **L2** resembles the Sierpinski triangle, whereas H_6**L3** has a radiant, geometrically different form. The backfolded molecules (**L1** and **L2**) can be deconstructed into tritopic subunits attached to the inner fragments (shown in green).

[a] School of Chemical Engineering and Light Industry, Guangdong University of Technology, Guangzhou 510006, Guangdong, China
[b] College of Chemistry, Fuzhou University, Fuzhou, Fujian 350108, China
[c] Department of Chemistry, City University of Hong Kong, 83 Tat Chee Avenue, Kowloon, Hong Kong, China. E-mail: zhengtao@cityu.edu.hk.
[d] Department of Chemistry, 560 Oval Drives, Purdue University, West Lafayette, Indiana, 47907 United States.
[e] Department of Chemistry, Hong Kong Baptist University, Waterloo Road, Hong Kong, China; HKBU Institute of Research and Continuing Education, Shenzhen Virtual University Park, Shenzhen, 518057, China. E-mail: rwywong@hkbu.edu.hk

† Electronic Supplementary Information (ESI) available: experimental details including synthetic procedures, NMR, IR, MS and elemental analysis data, cyclic voltammetry curve and tabulated crystallographic data. CCDC 1570192 contains the supplementary crystallographic data for **G2**. See DOI: 10.1039/x0xx00000x

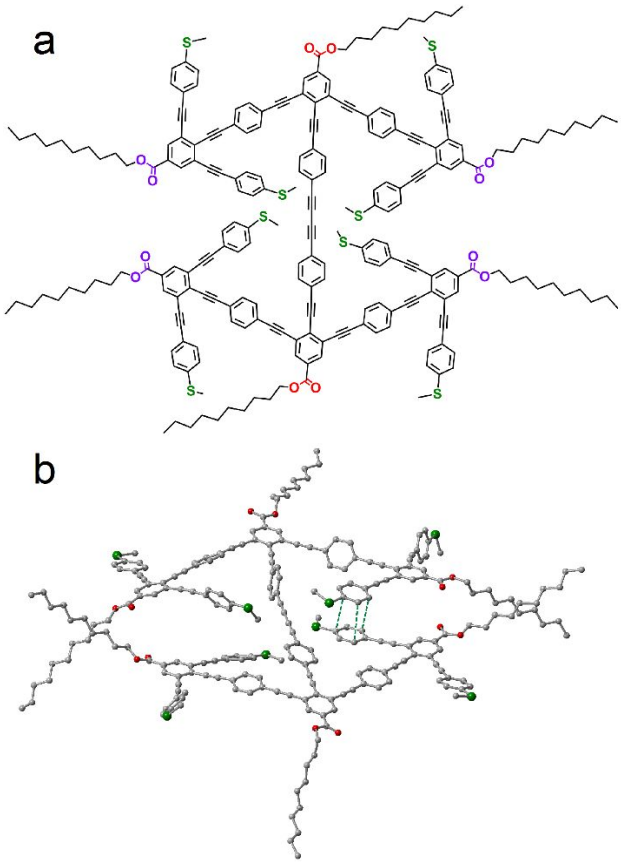

Fig. 2 a) A schematic model of molecule **G3**: a self-similar Sierpinski molecule featuring two carboxylate ester groups at the primary branch, together with six ester groups and 8 thioether groups at the secondary and tertiary branches, respectively. b) An energy-minimized conformation of molecule **G3**. Selected cofacial C···C contacts (3.438-3.643 Å) are shown by dashed lines. The geometry was optimized by classical molecular mechanics using the FORCITE package of the Materials Studio software. The Universal force field was selected, with the electrostatic and van der Waals terms being set as follows: Summation method: atom-based; Truncation method: cubic spline; Cutoff distance: 12.5 Å; Spline width: 1 Å; Buffer width: 0.5 Å.

primary branches and the –MeS units on the six secondary branches, with the backfolded configuration arranging the –MeS groups in three chelation pairs. The backfolded Sierpinski molecules have also proven interesting building blocks for extended networks, e.g., each molecule behaves as a collection of starburst units (e.g., the regular tritopic unit; see also **L1** and **L2** in Fig. 1); and the resultant networks, in spite of their unusual complexity, can be deconstructed into subnets corresponding to the starburst units of the molecule.[29]

To fill in the gap in the study of higher-generation Sierpinski molecules, and to draw more attention to this unconventional class of self-similar molecules, we here report the synthesis of molecule **G3** (Fig. 2). **G3** was designed with consideration to synthetic feasibility and functionality. For example, a total of six long alkyl groups (i.e., *n*-decyl, *n*-$C_{10}H_{11}$-) were installed at the (two) primary and (four) secondary termini to improve solubility; and extra phenylacetylene spacer units are built into the primary and secondary branches to alleviate steric hindrance. Also, the large, conjugated phenylene-acetylene backbone might help future studies on how the Sierpinski shape impacts photophysical properties (e.g., fluorescence/exciton lifetime, charge/energy transfer). In addition, the eight thioether groups at the **G3** branches can serve as metal-binding sites; while the long, floppy alkyl chains might also impart liquid crystal properties in combination with the rigid Sierpinski backbone.

Experimental

This is provided in the Supporting Information.

Results and discussion

The synthesis of **G3** builds on a convergent strategy extensively utilizing the well-established Sonogashira reaction,[30-36] in conjunction with the masking/demasking of the iodo and terminal alkyne groups by means of the triazene[37-40] and the trimethylsilyl (TMS) groups, respectively.[41] Among the many precursors, molecule **9** is a cornerstone for the overall assembly scheme. As shown in Fig. 3, the synthesis of **9** begins with a carboxylic acid (**2**) formation from 3,5-dibromo-4-iodobenzonitrile (**1**), followed by esterification with 1-decanol to give **4** in 80% yield (via the acid chloride **3**). Sonogashira cross-coupling of **4** with 1 equivalent of trimethylsilylacetylene (TMSA) selectively displaces the iodo group to provide **5** in 76% yield, indicating that the higher reactivity of the iodo group overrides the steric hindrance from the flanking Br atoms. The two Br- groups in **5** were then reacted with 2 equivalents of 4-triazenephenylacetylene (**S4**, see Fig. S1 for its preparation) at 90 °C to afford compound **6** in 60% yield. After unmasking the TMS group of **6** with tetrabutylammonium fluoride (TBAF), the resultant terminal alkyne compound **7** was coupled with the iodo compound **S5** to afford **8** in 56% yield. Heating **8** in methyl iodide at 120 °C in a sealed vessel then replaces the triazene units by the iodo groups, generating **9** in 75% yield.

With the key precursor **9** in hand, the assembly of **G3** becomes relatively straightforward, which involves installing the tertiary branches and a Glaser coupling that oxidatively homocouples the terminal alkyne (Fig. 4). Specifically, molecule **11** was prepared by coupling 4-ethynylthioanisole (**S8**) with the above-mentioned molecule **5** (followed by the removal of the

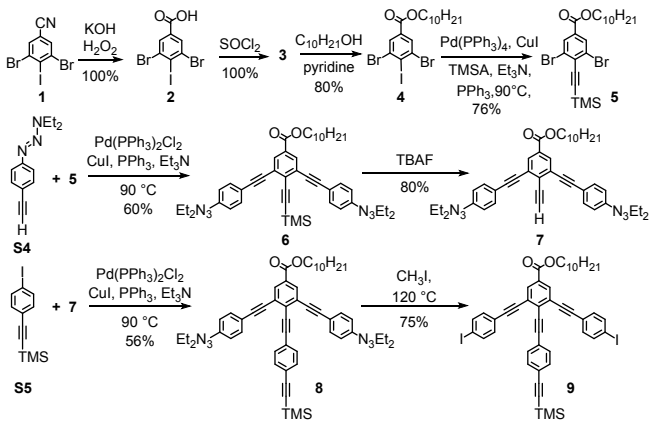

Fig. 3 The synthetic steps for molecule **9**.

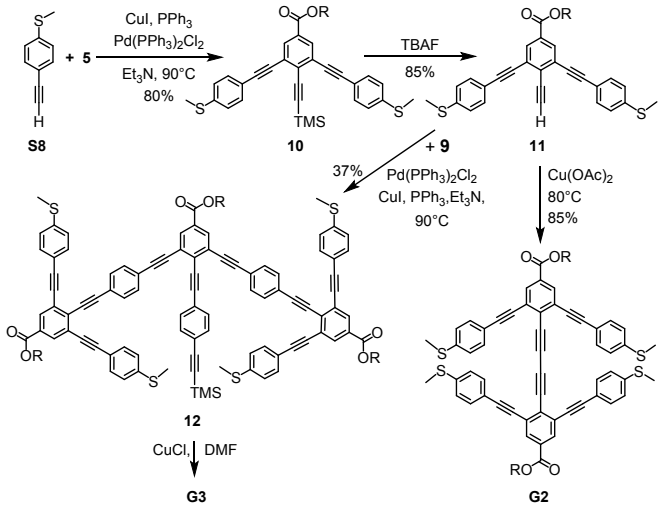

Fig. 4 Synthetic steps for **G3** and **G2** (R is an *n*-decyl group: *n*-$C_{10}H_{21}$-).

TMS group to recover the terminal alkyne function, with overall yields over 60%). Subsequently, **11** was subjected to a Sonogashira coupling with **9** to generate the precursor **12**. Notice however that the reaction between **11** and **9** required the rather stringent conditions of refluxing for 40 h, and the yield was modest (37%). Finally, compound **12** (without removing the TMS group) directly underwent a homocoupling reaction in the presence of CuCl in *N,N*-dimethylformamide (DMF) to afford the target **G3** as an orange solid in 52% yield.

The product **G3** was extensively characterized, e.g., by solution ^{1}H NMR, ^{13}C NMR, 2D COSY, DEPT spectra and cyclic voltammetry (Fig. S2 and elsewhere in ESI). In addition, high-resolution mass spectrometry HRMS found, e.g., 3478.4020 (100%) for M + H^+ (3478.435 calculated for $C_{234}H_{218}O_{12}S_8 + H^+$), and the CHN elemental analysis results are also consistent with the proposed structure, i.e., calculated for $C_{234}H_{218}O_{12}S_8$: C, 80.79; H, 6.32; found: C, 80.42; H, 6.57.

Table 1 Crystal Data and Structure Refinement Parameters for **G2**.

Compound	**G2**
Chemical Formula	$C_{74}H_{74}O_4S_4$
Formula weight	1155.57
Temperature (K)	100 (2)
Crystal size (mm)	0.50 × 0.17 × 0.10
Space group	*P* -1
a (Å)	8.960 (2)
b (Å)	11.752 (3)
c (Å)	15.156 (4)
α (°)	90.717 (4),
β (°)	103.972 (3)
γ (°)	92.265 (4)
V (Å^3)	1547.0 (6)
Z	1
ρ_{calcd} (g cm^{-1})	1.240
GOF	1.033
R_1[a] [I >2σ(I)]	0.0438
wR_2[b] [I >2σ(I)]	0.1037

$^{a}R_1=\sum(||F_o|-|F_c||)/\sum|F_o|$; $^{b}wR_2=[\sum w(F_o^2-F_c^2)^2/\sum w(F_o^2)^2]^{1/2}$

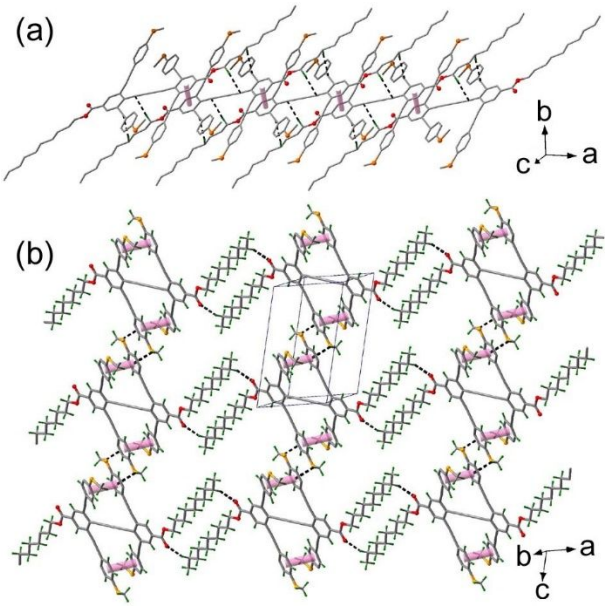

Fig. 5 A stack (panel a) and a layer (panel b) of molecules in the crystal structure of **G2**. The *π*···*π* interactions are shown as pink sticks and other intermolecular contacts are shown as black dotted lines. Color code: S, orange; O, red; C, grey.

For comparison, the lower generation Sierpinski molecule **G2** was synthesized (see Fig. 4 and ESI for the procedure). The **G2** crystal structure (space group *P*-1; Table 1) features the molecule in the achiral, *C*i-symmetric butterfly conformation (cf. the C_2-symmetric, dihedral conformation found in a related system[1], see Fig. S3 for the butterfly and dihedral atropisomers). The side-arm phenyl units from the two butterfly halves of **G2** form face-to-face overlaps with C···C (e.g., 3.421 and 3.500 Å) and C···S (e.g., 3.669 Å) contacts. The molecules of **G2** stack along the crystallographic *a* axis: the neighboring molecules are significantly offset (i.e., slipped by 67.5°), with face-to-face contacts between the backbone phenylacetylene units (e.g., C···C distances: 3.315 and 3.433 Å; Fig. 5a). The **G2** stacks as such were aligned along the *c* axis to form layers of the aromatics, with distinct C···S (3.811 Å) interactions across the individual stacks. The layers are piled along the *b* axis, with dimeric aggregates of the long aliphatic chains found in-between (Fig. 5b). Across the layers, no short contacts were observed between the aromatics and the S···S distance (4.259 Å) is also well above the VDW diameter of sulfur (3.6 Å). The lamellar character (along the *b* or 010 plane) is also reflected in the intensity profile of the PXRD patterns (Fig. 6), as in the weakened 001 peak relative to the 010 peak.

A comparison of the solution UV-vis absorption and emission spectra of **G2** and **G3** (Fig. 7) unveils some surprises. The UV-vis wavelengths of maximum absorption (λ_{max}) of conjugated systems generally arise from *π*→*π** transitions from the HOMO to the LUMO, and often red-shift significantly with added conjugation. In spite of the larger π-electron backbone of **G3**, its λ_{max} is, surprisingly close to that of **G2** (with $\lambda_{max,G3}$ = 328 nm and $\lambda_{max,G2}$ = 320 nm; Fig. 7a; molar extinction coefficients: ε_{G3} = 2.1x10^5; ε_{G2} = 8.03x10^4 M^{-1}cm^{-1}). A bathochromic side band (most likely from *n*→*π** transitions) was also observed for both

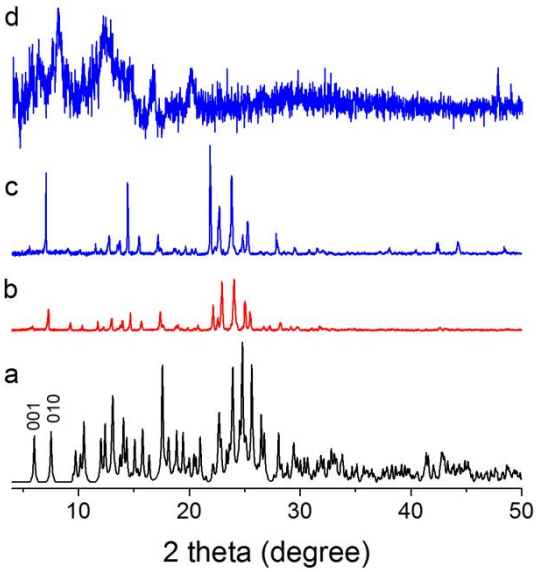

Fig. 6 X-ray powder patterns (Cu Kα, λ=1.5418 Å): (a) calculated from the single crystal structure of **G2**; (b) a powder sample obtained from rotary-evaporating a dichloromethane solution of **G2**; (c) a ground crystal sample--the crystals were obtained by slowly evaporating a dichloromethane (e.g., 3.0 mL) solution of **G2** (e.g., 15 mg); (d) a powder sample of **G3** obtained from slowly diffusing acetonitrile (1.0 mL) into a toluene (2.0 mL) solution of **G3** (10 mg) in glass tube (diameter: 8.0 mm) over three days. The pattern was measured on a Rigaku SmartLab X-ray diffractometer operating at 40 kV, 30 mA, and a scan rate of 10 °/min.

cases, with the absorption edge of **G2** slightly red-shifted relative to the larger **G3**. Unexpected observations continue in the fluorescent spectra. In THF, the small **G2** exhibits a broad emission peaked at 516 nm, while **G3** exhibits a major emission at 498 nm and a broad shoulder at about 525 nm: as shown in Fig. 7b, the emission profile of **G2** is red-shifted relative to **G3**.

G2 solid samples from various solvents/conditions form the same crystalline phase (e.g., Fig. 7, patterns b and c), and their emission spectra (e.g., Fig. 7b; with two close peaks with λ_{max}= 510 and 525 nm) are similar to that of the solution sample. The persistent crystalline phase of **G2** (e.g., even in fast precipitation from the rotary evaporator; as revealed by the PXRD pattern of Fig. 6c) can be understood in light of the stacking and packing forces unveiled from the above-mentioned single crystal structure (Fig. 5). In particular, the distinct π-π interactions between the side-arm phenyl units help to forge the well-defined, rigid conformation of the **G2** molecules; the intermolecular π-π as well as CH-π interactions, on the other hand, direct the packing motif of their super-structure in the solid state.

By contrast, the solid samples of the more complex **G3**, however, exhibits poor crystallinity—even in solid samples obtained from carefully controlled diffusion experiments (Fig. 6, pattern d). The resistance of **G3** molecules against crystallization can be rationalized by the complex branched structure, which allows many energetically similar conformations to exist both in solution and in the solid state, thereby frustrating periodic ordering in the aggregates of the **G3** molecules. For illustrating the diverse and flexible conformations of **G3**, the computationally optimized geometry of **G3** (see Fig. 2, panel b) is informative. In particular, the conformation in Fig. 2b feature a pair of cofacially-stacked bezenoid units of the tertiary branches; but, unlike the decidedly rigidifying cofacial pairs in the smaller **G2** molecule (Fig. 5b), the cofacial pair here does not prevent the rotation of the side arms in the larger structure of **G3** (e.g., the secondary branches can readily turn, and pull the pair apart, as is in the case of the left moiety of the **G3** molecules in Fig. 2b). Also, the more numerous and irregularly arranged alkyl chains of **G3** molecules further complicate the packing motifs of the molecules to disfavor the ordered array required by crystallization.

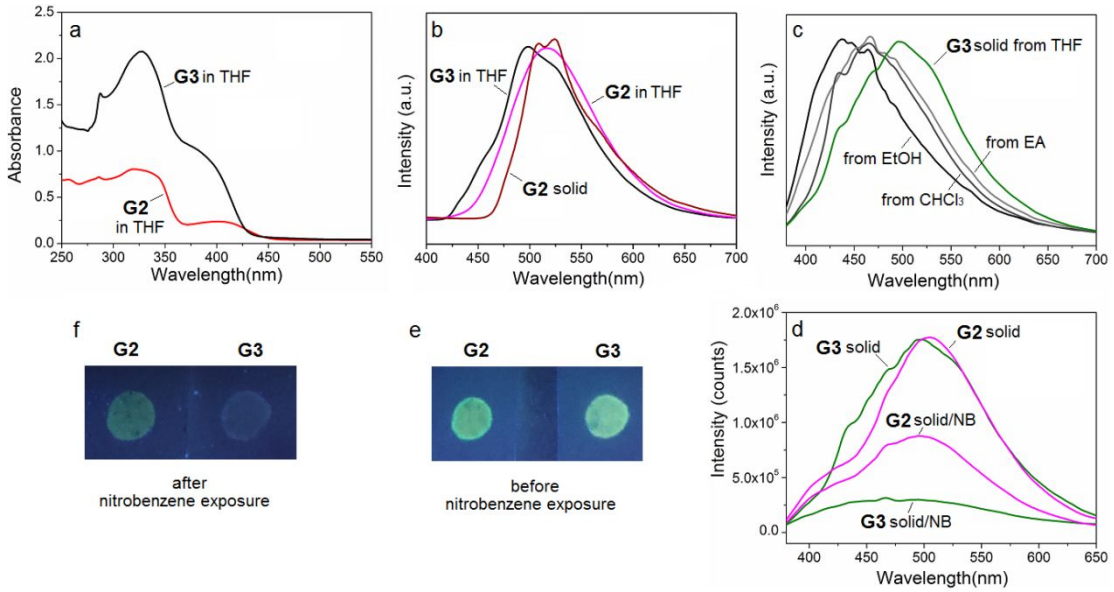

Fig. 7 (a) UV-vis spectra of **G2** (red graph) and **G3** (black graph) in THF (10^{-5} M; slit width: 20 nm); (b) Emission spectra of **G2** in THF (λ_{ex}= 360 nm), **G2** in the solid state (λ_{ex}= 380 nm), **G3** in THF (λ_{ex}= 380 nm); (c) Emission spectra of **G3** solid samples deposited from THF, ethyl acetate (EA), $CHCl_3$ and ethanol (λ_{ex}= 360 nm); (4) Emission spectra of **G2** and **G3** solid samples (both deposited from THF) before and after nitrobenzene (NB) exposure (λ_{ex}= 360 nm), with corresponding photographs of the samples under UV radiation (λ= 365 nm) shown in panels (e) and (f), respectively. Slit width for excitation beam: 2 nm.

As the luminescent characteristics of the molecules closely depend on their conformations as well as the intermolecular arrangements, the highly changeable emission features as observed of **G3** molecules in the solid state (Fig. 7c) are not unexpected. For example, their emission features depend on the solvents used for deposition. As shown in Fig. 7c, the solid sample from THF fluoresces at distinctly longer wavelengths (relative to other solvents). The variable solid state emission profiles of **G3** can be (tentatively) ascribed to the diverse packing motifs engendered by its complex branched shape. On the other hand, the absence of red shift in the solution spectra of **G3** (relative to the much smaller **G2**) runs counter to the general trend of higher-generation dendrimers to absorb and emit at longer wavelengths[42-44] (albeit to a lesser degree for meta-conjugated systems[45, 46]). We suspect that the diacetylene bridge in **G2** offers an efficient push-pull pathway between the sulfur and the carboxyl groups to facilitate π-electron delocalization, while such a push-pull effect becomes weaker in the longer, zigzag path offered by **G3** (see Fig. S4). Further studies on the excitation dynamics of Sierpinski molecules are needed for elucidating the unexpected absence of red shift observed in the solution spectra of **G3**, and for uncovering other potentially interesting photophysical properties.

The complex branched shape of **G3** may also account for its enhanced sensitivity to nitrobenzene (e.g., by allowing for easier guest penetration into the solid). As shown in Fig. 7d-f, the fluorescence of the **G3** thin film (drop-cast onto filter paper from a THF solution: 0.3 mg/mL; 1.0 μL) was largely quenched after being suspended over nitrobenzene in a capped vial (e.g., at 80 °C for 5 minutes); by comparison, a **G2** thin film (similarly cast from THF: 0.3 mg/mL; 1.0 μL) shows lesser fluorescence quenching, as is both visually and spectroscopically observed.

Conflicts of interest

There are no conflicts to declare.

Acknowledgements

This work was supported by an SRG grant of City University of Hong Kong (Project 7004820), the National Natural Science Foundation of China (21871061), Local Innovative and Research Teams Project of Guangdong Pearl River Talents Program and Science and Technology Program of Guangzhou (201807010026). W.-Y.W. thanks the financial support from Hong Kong Research Grants Council (HKBU 12302114). M.Z. thanks the United States National Science Foundation (Grant CHE 0087210), Ohio Board of Regents Grant CAP-491, and Youngstown State University for funding for the single crystal diffractometer.

Notes and references

1. Y.-Q. Sun, J. He, Z. Xu, G. Huang, X.-P. Zhou, M. Zeller and A. D. Hunter, *Chem. Commun.*, 2007, 4779-4781.
2. Z. Xu, Y.-Q. Sun, J. He, M. Zeller and A. D. Hunter, in *The concept and use of a class of branchy molecules with centripetal self-similarity*, Nova Science Publishers, Inc., Hauppauge, NY 2008.
3. Y.-Q. Sun, C. Yang, Z. Xu, M. Zeller and A. D. Hunter, *Cryst. Growth Des.*, 2009, **9**, 1663-1665.
4. J. He, M. Zeller, A. D. Hunter and Z. Xu, *CrystEngComm*, 2015, **17**, 9254-9263.
5. J. Cui, Y.-L. Wong, M. Zeller, A. D. Hunter and Z. Xu, *Angew. Chem., Int. Ed.*, 2014, **53**, 14438-14442.
6. C. R. Woods, M. Benaglia, S. Toyota, K. Hardcastle and J. S. Siegel, *Angew. Chem. Int. Ed.*, 2001, **40**, 749-751.
7. R. Nandy, M. Subramoni, B. Varghese and S. Sankararaman, *J. Org. Chem.*, 2007, **72**, 938-944.
8. V. Narayanan, S. Sankararaman and H. Hopf, *Eur. J. Org. Chem.*, 2005, 2740-2746.
9. J. A. Marsden, M. J. O'Connor and M. M. Haley, *Org. Lett.*, 2004, **6**, 2385-2388.
10. J. D. Bradshaw, L. Guo, C. A. Tessier and W. J. Youngs, *Organometallics*, 1996, **15**, 2582-2584.
11. M. Laskoski, W. Steffen, J. G. M. Morton, M. D. Smith and U. H. F. Bunz, *J. Organomet. Chem.*, 2003, **673**, 25-39.
12. W. Yang, G. Longhi, S. Abbate, A. Lucotti, M. Tommasini, C. Villani, V. J. Catalano, A. O. Lykhin, S. A. Varganov and W. A. Chalifoux, *J. Am. Chem. Soc.*, 2017, **139**, 13102-13109.
13. E. Buhleier, W. Wehner and F. Vögtle, *Synthesis*, 1978, 155-158.
14. D. A. Tomalia, A. M. Naylor and W. A. Goddard, III, *Angew. Chem.*, 1990, **102**, 119-157.
15. J. S. Moore, *Acc. Chem. Res.*, 1997, **30**, 402-413.
16. A. W. Bosman, H. M. Janssen and E. W. Meijer, *Chem. Rev.*, 1999, **99**, 1665-1688.
17. C. C. Lee, J. A. MacKay, J. M. J. Fréchet and F. C. Szoka, *Nat. Biotechnol.*, 2005, **23**, 1517-1526.
18. M. Gingras, J.-M. Raimundo and Y. M. Chabre, *Angew. Chem. Int. Ed.*, 2007, **46**, 1010-1017.
19. S.-H. Hwang, C. D. Shreiner, C. N. Moorefield and G. R. Newkome, *New J. Chem.*, 2007, **31**, 1192-1217.
20. M. Kozaki, S. Morita, S. Suzuki and K. Okada, *J. Org. Chem.*, 2012, **77**, 9447-9457.
21. G. R. Newkome, P. Wang, C. N. Moorefield, T. J. Cho, P. P. Mohapatra, S. Li, S.-H. Hwang, O. Lukoyanova, L. Echegoyen, J. A. Palagallo, V. Iancu and S.-W. Hla, *Science*, 2006, **312**, 1782-1785.
22. P. W. K. Rothemund, N. Papadakis and E. Winfree, *PLoS Biol.*, 2004, **2**, 2041-2053.
23. J. Shang, Y. Wang, M. Chen, J. Dai, X. Zhou, J. Kuttner, G. Hilt, X. Shao, J. M. Gottfried and K. Wu, *Nat. Chem.*, 2015, **7**, 389-393.
24. D. Nieckarz and P. Szabelski, *Chem. Commun.*, 2016, **52**, 11642-11645.
25. X. Zhang, N. Li, G.-C. Gu, H. Wang, D. Nieckarz, P. Szabelski, Y. He, Y. Wang, C. Xie, Z.-Y. Shen, J.-T. Lu, H. Tang, L.-M. Peng, S.-M. Hou, K. Wu and Y.-F. Wang, *ACS Nano*, 2015, **9**, 11909-11915.
26. G. Gu, N. Li, L. Liu, X. Zhang, Q. Wu, D. Nieckarz, P. Szabelski, L. Peng, B. K. Teo, S. Hou and Y. Wang, *RSC Adv.*, 2016, **6**, 66548-66552.
27. X. Zhang, N. Li, L. Liu, G. Gu, C. Li, H. Tang, L. Peng, S. Hou and Y. Wang, *Chem. Commun.*, 2016, **52**, 10578-10581.
28. N. Li, G. Gu, X. Zhang, D. Song, Y. Zhang, B. K. Teo, L.-m. Peng, S. Hou and Y. Wang, *Chem. Commun.*, 2017, **53**, 3469-3472.
29. C. Yang, Y.-L. Wong, R. Xiao, M. Zeller, A. D. Hunter, S.-M. Yiu and Z. Xu, *ChemistrySelect*, 2016, **1**, 4075-4081.
30. Z. Luo, N. Zhu and D. Zhao, *Chem. - Eur. J.*, 2016, **22**, 11028-11034.
31. D. Zhao and J. S. Moore, *Chem. Commun.*, 2003, 807-818.
32. Y. Jin, Q. Wang, P. Taynton and W. Zhang, *Acc. Chem. Res.*, 2014, **47**, 1575-1586.
33. R. Chinchilla and C. Najera, *Chem. Rev.*, 2007, **107**, 874-922.
34. R. Chinchilla and C. Najera, *Chem. Soc. Rev.*, 2011, **40**, 5084-5121.
35. N. M. Jenny, M. Mayor and T. R. Eaton, *Eur. J. Org. Chem.*, 2011, **2011**, 4965-4983.
36. A. M. Thomas, A. Sujatha and G. Anilkumar, *RSC Adv.*, 2014, **4**, 21688-21698.
37. D. B. Kimball and M. M. Haley, *Angew. Chem., Int. Ed.*, 2002, **41**, 3338-3351.
38. Y. Zhang, D. Cao, W. Liu, H. Hu, X. Zhang and C. Liu, *Curr. Org. Chem.*, 2015, **19**, 151-178.
39. Z. Wu and J. S. Moore, *Tetrahedron Lett.*, 1994, **35**, 5539-5542.
40. B. T. Holmes, W. T. Pennington and T. W. Hanks, *Synth. Commun.*, 2003, **33**, 2447-2461.
41. Z. Xu, M. Kahr, K. L. Walker, C. L. Wilkins and J. S. Moore, *J. Am. Chem. Soc.*, 1994, **116**, 4537-4550.
42. J. S. Melinger, Y. Pan, V. D. Kleiman, Z. Peng, B. L. Davis, D. McMorrow and M. Lu, *J. Am. Chem. Soc.*, 2002, **124**, 12002-12012.
43. Z. Peng, Y. Pan, B. Xu and J. Zhang, *J. Am. Chem. Soc.*, 2000, **122**, 6619-6623.
44. M. Lu, Y. Pan and Z. Peng, *Tetrahedron Lett.*, 2002, **43**, 7903-7906.
45. K. M. Gaab, A. L. Thompson, J. Xu, T. J. Martinez and C. J. Bardeen, *J. Am. Chem. Soc.*, 2003, **125**, 9288-9289.
46. R. Kopelman, M. Shortreed, Z.-Y. Shi, W. Tan, Z. Xu, J. S. Moore, A. Bar-Haim and J. Klafter, *Phys. Rev. Lett.*, 1997, **78**, 1239-1242.